



Optimization of data acquisition parameters for single gamma line sensing: $\text{KSr}_2\text{I}_5:\text{Eu}^{2+}$ and $\text{NaI}(\text{Tl})$ compared

Eric Lukosi ^{a,b,*}, Mikah Rust ^{a,b}, Luis Stand ^{c,d}, Charles L. Melcher ^{a,c,d}

^a Department of Nuclear Engineering, University of Tennessee, 37996, United States

^b Joint Institute for Advanced Materials, University of Tennessee, 37996, United States

^c Scintillation Materials Research Center, University of Tennessee, 37996, United States

^d Department of Materials Science and Engineering, University of Tennessee, 37996, United States

ARTICLE INFO

Keywords:

KSr₂I₅
KSI
Gamma spectroscopy
Radiation detection
Time-to-detection

ABSTRACT

$\text{KSr}_2\text{I}_5:\text{Eu}^{2+}$ scintillators exhibit better than 3% energy resolution at 662 keV and may be significantly less expensive to produce than other, similar energy resolution scintillators. However, $\text{KSr}_2\text{I}_5:\text{Eu}^{2+}$ exhibits a 6.5 Bq/cm³ intrinsic background from the presence of ⁴⁰K. This background is not only the well-known 1.46 MeV gamma, but also the 1.31 MeV end point of the beta spectrum. This paper computationally evaluates the optimum data acquisition parameters of $\text{KSr}_2\text{I}_5:\text{Eu}^{2+}$ and compares them to $\text{NaI}(\text{Tl})$ for the detection of single line gamma sources between 0.01–2.2 MeV with incident source strengths between 5 s⁻¹ and 100 s⁻¹ striking the detector. We found a strong dependence of the time-to-detection on the data acquisition parameters, where the time-to-detection of $\text{KSr}_2\text{I}_5:\text{Eu}^{2+}$ was 1–3 times larger than $\text{NaI}(\text{Tl})$ across the parameter space. The largest discrepancy observed was between 0.6 MeV and 1.2 MeV, where the intrinsic 1.31 MeV beta dominates the background.

1. Introduction

A new scintillator, $\text{KSr}_2\text{I}_5:\text{Eu}^{2+}$, or KSI, is under development as a low-cost, high-energy resolution radiation sensor. Literature suggests that KSI may be grown at several mm per hour with high yield and requires only inexpensive source materials [1,2]. The combination of low cost and decent energy resolution would be valuable to the detection of radioisotopes, as the detector energy resolution has been shown to be critical [3,4]. However, the presence of ⁴⁰K results in an intrinsic radioactivity of ~6.5 Bq/cm³. The decay of ⁴⁰K results in beta emission 89.25% of the time and a 1.46 MeV gamma ray via electron capture 10.55% of the time [5]. The beta particle has a maximum energy of 1.31 MeV and peaks at 560 keV. Currently, it is unclear what effect the intrinsic radioactivity of KSI will have on its performance in detecting weak gamma-emitting sources.

While high energy resolution scintillators like $\text{SrI}_2:\text{Eu}^{2+}$ [6,7] and $\text{LaBr}_3:\text{Ce}^{3+}$ [8,9] are available with no, or a much reduced, intrinsic radioactivity, respectively, they are considerably more expensive than $\text{NaI}(\text{Tl})$. While KSI will likely never be as inexpensive as $\text{NaI}(\text{Tl})$, its apparent faster growth rate and yield suggests it should be cheaper than its lower intrinsic background counterparts [10,11]. For this reason, we report here on the first computational evaluation of the effect of the intrinsic radioactivity of KSI on the time it takes to detect single line gamma rays. Specifically, the data acquisition parameters were

systematically evaluated over a range of gamma ray energies and source strengths to identify the lowest time-to-detection (TTD) of single gamma lines and compare the results to a standard $\text{NaI}(\text{Tl})$ using the same methodology.

2. Methods

Comparison of the single gamma line sensing capabilities of KSI compared to $\text{NaI}(\text{Tl})$ is evaluated through using a region of interest around each gamma line [12]. The minimum TTD is computationally evaluated through a systematic evaluation of these data acquisition parameters: boxcar sum window (BCS), integration window around the gamma energy (referred here on as integration window), and false positive rate (FPR). Each scintillator is assumed to sample the number of counts observed from the source and background at a frequency of 10 Hz. The background utilized in the computations were experimentally measured using 10×1 inch cylindrical KSI and $\text{NaI}(\text{Tl})$ scintillators coupled to a Hamamatsu 6231 PMT (see Fig. 1). The size of each cylindrical scintillator was 10×1 inch. The gamma energy range simulated for both KSI and $\text{NaI}(\text{Tl})$ was between 0.01–2.2 MeV, in steps of 0.005 MeV. The intrinsic efficiency of each scintillator was simulated using MCNP6 [13] and the pulse height light tally to determine the rate of full energy deposition (i.e., photopeak efficiency).

* Corresponding author at: Department of Nuclear Engineering, University of Tennessee, 37996, United States.

E-mail address: elukosi@utk.edu (E. Lukosi).

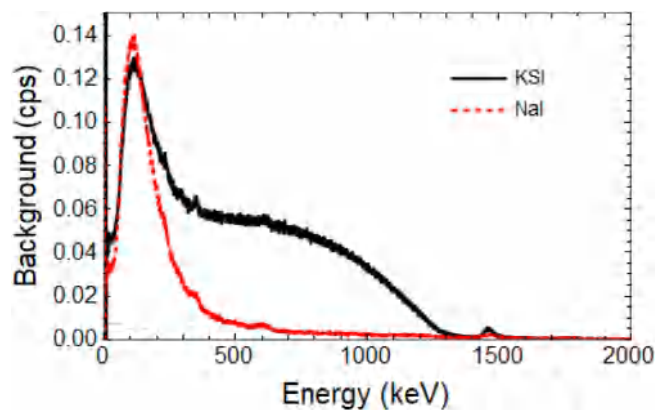


Fig. 1. Experimentally measured background of KSI and NaI(Tl). The energy bin width is 0.6 keV for KSI and 0.7 keV for NaI(Tl). The number of bins is 4096 for each spectrum.

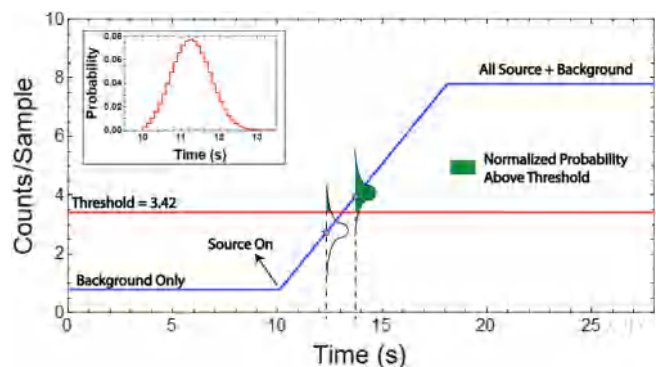


Fig. 2. Expected average signal of KSI for a source strength striking the detector (sps) of 20 s^{-1} , gamma energy of 1.5 MeV, BCS of 8 s, FPR of 0.01%, and peak integration window of $\pm 0.95\sigma$. Overlaid on the image is a graphical depiction of an assumed Gaussian distribution of observed counts at each sample, where the green shaded region corresponds to the probability that the observed number of counts in that sample will pass the threshold. The inset on the top left is the corresponding sequential difference of the normalized probability of sample “i” passing the threshold.

The MCNP6 simulations assumed a plane wave of incident gammas on the front face of each 1×1 inch cylindrical scintillator. The plane wave nature of the source removes the geometric dependency of the results on detector–source separation distances several times greater than the diameter/length of the detector. The source radiation strikes per second (sps) on the detector varied between 5 sps and 100 sps.

Rather than utilizing a single interval test, the TTD is evaluated with an equal distribution of background and source plus background time intervals plus twice the time width of the BCS. Instead of simulating thousands of randomly generated background and source counts per parameter space, we rely on the fact that using the average number of background and source counts expected at each sample will produce the same result as the number of simulations approach infinity. The BCS is defined as the sum of counts observed over some time interval, as described in Eq. (1). Here, the expected gross count rate within the integration window, C_i , for each sample is summed backward in time to the evaluated window, z_{mov} , yielding a total observed count of C_z . In these simulations, the background count rate is flat before the source is turned on, at which point the observed counts exhibits a constant rate of increase until the BCS is entirely over the source plus background region of the dataset (see Fig. 2).

$$C_z = \sum_{i=z_{\text{mov}}-1}^0 C_i \quad (1)$$

The threshold C_{th} , defined in Eq. (2), is dependent on the FPR, where C_B is the average background rate expected for a given parameter space. The multiplier M was found by utilizing the cumulative Binomial probability distribution and requiring that the probability of observing two or more samples above the threshold in ten sequential samples is equal to the desired FPR. The FPR was evaluated at both 1% and 0.01%.

$$C_{\text{th}} = C_B (1 + M) \quad (2)$$

The number of observed counts per sample from each scintillator at each gamma energy and source strength was determined by summing over different areas of the photopeak region. Each photopeak was assumed to be Gaussian, and the integration window varied between $\pm 0.25\sigma$ and $\pm 4\sigma$, in steps of 0.05σ . The width parameter σ was found using the detector energy resolution (E_R) at 662 keV ($E_{R,\text{SKI}} = 3.5\%$; $E_{R,\text{NaI(Tl)}} = 6.5\%$) and appropriately scaled using their known resolution curves at each simulated gamma energy. The BCS varied between 10 and 150 samples (1 s to 15 s). The overlap of the observed counts at each sample with the FPR threshold defines the probability P_z of each sample causing a gamma source detection event. This is graphically displayed in Fig. 2 via the shaded area underneath the two Gaussian curves. Taking the sequential difference of the normalized P_z , the most probable sample position (i.e., TTD) when the source is detected is found. The reported TTD is the minimum value found across the simulated integration window ($\pm\sigma$) for a given parameter space. To summarize, the simulated parameter space in this report is the BCS (1 s to 15 s), gamma source energy (0.01 MeV to 2.2 MeV), sps (2.5 s^{-1} to 100 s^{-1}), integration window ($\pm 0.25\sigma$ to $\pm 4\sigma$), and FPR (1% and 0.01%).

3. Results

While the output of this computational study is extensive, we present a quantitative comparison between KSI and NaI(Tl) for two different source strengths (15 s^{-1} and 50 s^{-1}). The output presented is the optimum integration window that minimizes the TTD for each parameter space and the corresponding ratio of the TTD of KSI to NaI(Tl). The former is important in defining the optimum data acquisition parameters for weak source detection using single gamma lines, valuable in developing more complex isotope identification algorithms. The latter provides a quantitative comparison of the effect of the intrinsic background of KSI on single gamma line sensing compared to NaI(Tl).

In Fig. 3, the optimum integration window that minimizes the TTD for 15 sps is provided. The optimum integration window for KSI is roughly equal to NaI(Tl) for low gamma energies, but becomes a little larger in the region where the 1.31 MeV beta dominates the background for larger moving windows. This is due to the interplay between the source-to-background (S/N) ratio, threshold C_{th} , and the normalized sequential difference of the probability P_z that minimizes the TTD. As an example, the background and source (photopeak) count rates as well as the threshold C_{th} at an integration window of $\pm 1\sigma$ and $\pm 1.3\sigma$ is provided in Table 1 for an incident 662 keV gamma ray at a source strength of 15 sps with a BCS of 1 s. In evaluating the data, the poorer energy resolution of NaI(Tl) results in a large observed increase in the background rate of 31.3%, which is mostly compensated by the large 30.4% increase observed for KSI due to its dominant internal background from the 1.31 MeV beta particle around 662 keV. The source rate for NaI(Tl) and KSI increases as the integration window increases by 18.2% and 17.7%, and C_{th} increases by 17.4% and 19.9%, respectively. From the observed changes, it would seem that the optimum integration window between these two options would be $\pm 1\sigma$ for KSI. However, the increase in source rate results in more overlap of the gross count rate C_z with C_{th} as the boxcar window moves across the point in time when the source is turned on, resulting in a faster TTD (see Fig. 2). Obviously, as the integration window

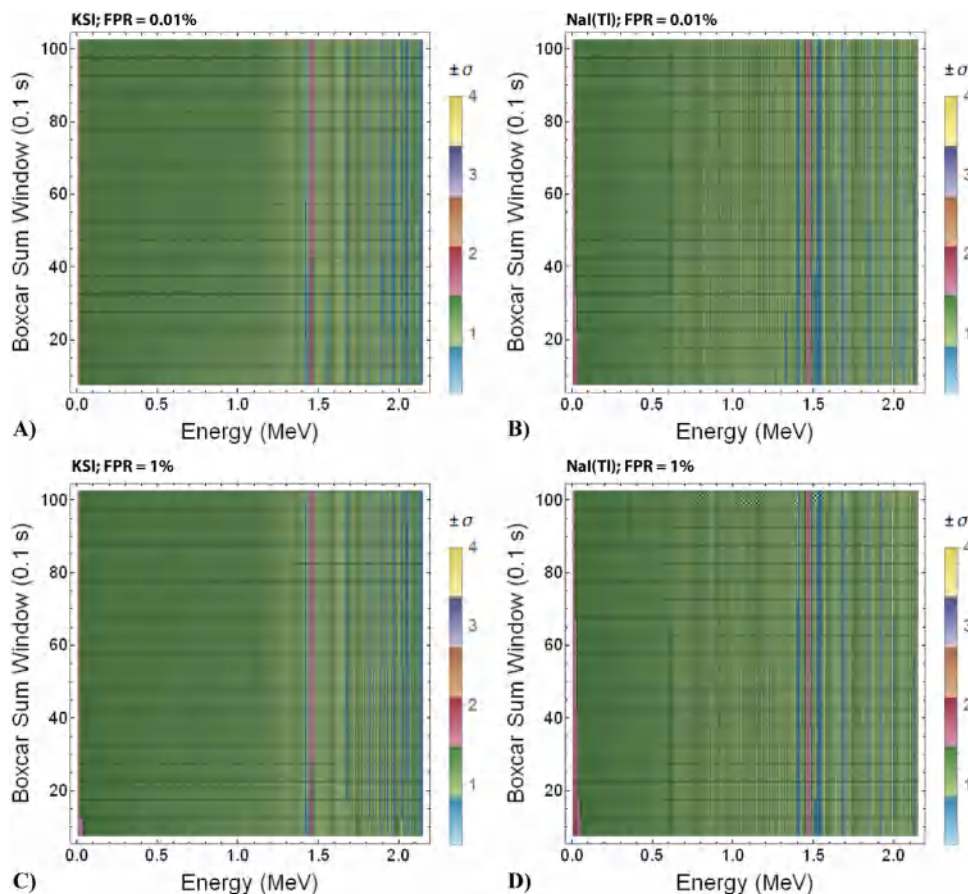


Fig. 3. Optimum integration window of KSI ((A) and C) and NaI (B) and D) as a function of energy and box car sum (BCS) at 15 sps for a FPR of 0.01% (A–B) and 1% (C–D)). The optimum integration window that minimizes the TTD in the chosen parameter space is larger for KSI than NaI(Tl) due to the need to optimize the S/N ratio in the region where the 1.31 MeV end point energy beta from ^{40}K decay dominates the background spectrum of KSI. The blue vertical lines above 1.5 MeV are due to the transition between green and blue color bar legend regions and the effect of the low probability, high energy background gammas have on the optimum integration window. (For interpretation of the references to color in this figure legend, the reader is referred to the web version of this article.)

Table 1

Background and source (photopeak) count rates at two different integration windows for a 662 keV source strength of 15 sps and a BCS of 1 s. Also included is the associated threshold C_{th} used to evaluate the TTD for the data acquisition parameters.

| Detector | C_B (cps) | | Source (Photopeak) rate (cps) | | C_{th} (cps) | |
|----------|---------------|-----------------|-------------------------------|-----------------|----------------|-----------------|
| | $\pm 1\sigma$ | $\pm 1.3\sigma$ | $\pm 1\sigma$ | $\pm 1.3\sigma$ | $\pm 1\sigma$ | $\pm 1.3\sigma$ |
| NaI(Tl) | 0.16 | 0.21 | 1.87 | 2.21 | 1.02 | 1.20 |
| KSI | 1.61 | 2.10 | 2.03 | 2.39 | 4.36 | 5.23 |

continues to increase, the source rate increases at an ever slower rate compared to the background, resulting in C_{th} increasing to a degree that the TTD becomes larger. It is this interplay that has been optimized and presented in Fig. 3.

A two dimensional plot of the optimum integration window at 15 sps and 50 sps and a BCS of 1.5 s and 10 s at a FPR of 0.01% in Fig. 4 better illustrates the optimum integration window trend across the simulated source energies. In agreement with the aforementioned example, as the sps increases, the difference between the optimum integration window for KSI and NaI(Tl) in the 0.5–1.3 MeV range becomes less pronounced, and both shift upward slightly. Of note is the large increase in optimum integration window around 1.46 MeV, which is the gamma energy from ^{40}K decay present in the background observed by both NaI(Tl) and KSI. The width of the band observed in Fig. 3 is larger for NaI(Tl) than KSI, which is a consequence of the better energy resolution of KSI. Finally, the effect of the FPR on the optimum integration window is minimal, varying on average by just a few step sizes ($\pm 0.05\sigma$) across the parameter space.

The KSI-to-NaI(Tl) TTD ratio is provided in Fig. 5, where it is apparent that the internal 1.31 MeV beta of KSI increases the TTD by several multiples. For a sps of 15 s^{-1} and a FPR of 0.01%, the TTD of KSI is two-to-three times larger than NaI(Tl) between 0.6–1.1 MeV, but decreases somewhat as the BCS window increases. For larger source strengths, the difference in the TTD between KSI and NaI(Tl) is less sensitive to the BCS. Additionally, the TTD ratio increases slightly as the BCS window width increases at a source strength of 50 s^{-1} , opposite of that observed at a source strength of 15 s^{-1} . Further, as the required FPR is reduced, the difference in TTD between NaI(Tl) and KSI is much less pronounced, but the same general trends in sps are observed.

Increasing the BCS increases the source-to-background count ratio as the window moves across the time domain. However, having a large window also results in a slower response of the system, where the TTD for a single gamma line at 1 MeV increases from 1.9 s to 3.6 s for KSI when the BCS width increases from 1.5 s to 10 s at a sps of 15 s^{-1} and a FPR of 0.01% (see Fig. 6). For NaI(Tl), the TTD increases from 0.6 s to 1.4 s with the same change in parameter space. Further, the increase in the TTD ratio as the BCS increases at a sps of 50 s^{-1} indicates that there is an overall minimum TTD ratio for the combination of BCS and sps. Above 1.5 MeV, KSI exhibits a better TTD than NaI(Tl), which is outside the range of the intrinsic background from ^{40}K and is a consequence of the greater stopping power and better energy resolution of KSI. While a smaller BCS results in a faster TTD in all cases for both scintillators, it is also subject to more random noise. Although this source of uncertainty was not a subject of this investigation, a balance is required between the optimum data acquisition parameters and the actual TTD for a given application.

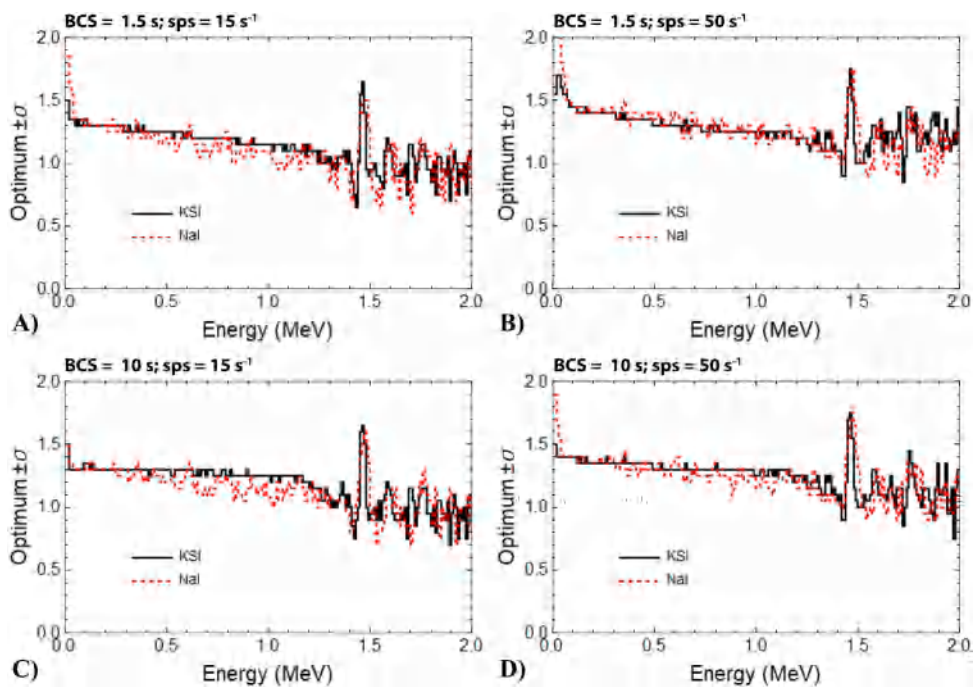


Fig. 4. Optimum integration window of KSI and NaI(Tl) for a BCS of 1.5 s (A)–(B) and 10 s (C)–(D) and a sps of 15 s⁻¹ (A) and (C) and 50 s⁻¹ (B) and (D) at a FPR of 0.01%. Here it can be observed that the optimum integration window of both KSI and NaI(Tl) are very similar, with KSI being slightly larger than NaI(Tl) for the lower sps of 15 s⁻¹ and in the region where the 1.31 MeV end point energy beta from ⁴⁰K decay dominates the overall background of KSI. Further, increasing the BCS results in additional separation of the optimum integration window between the two.

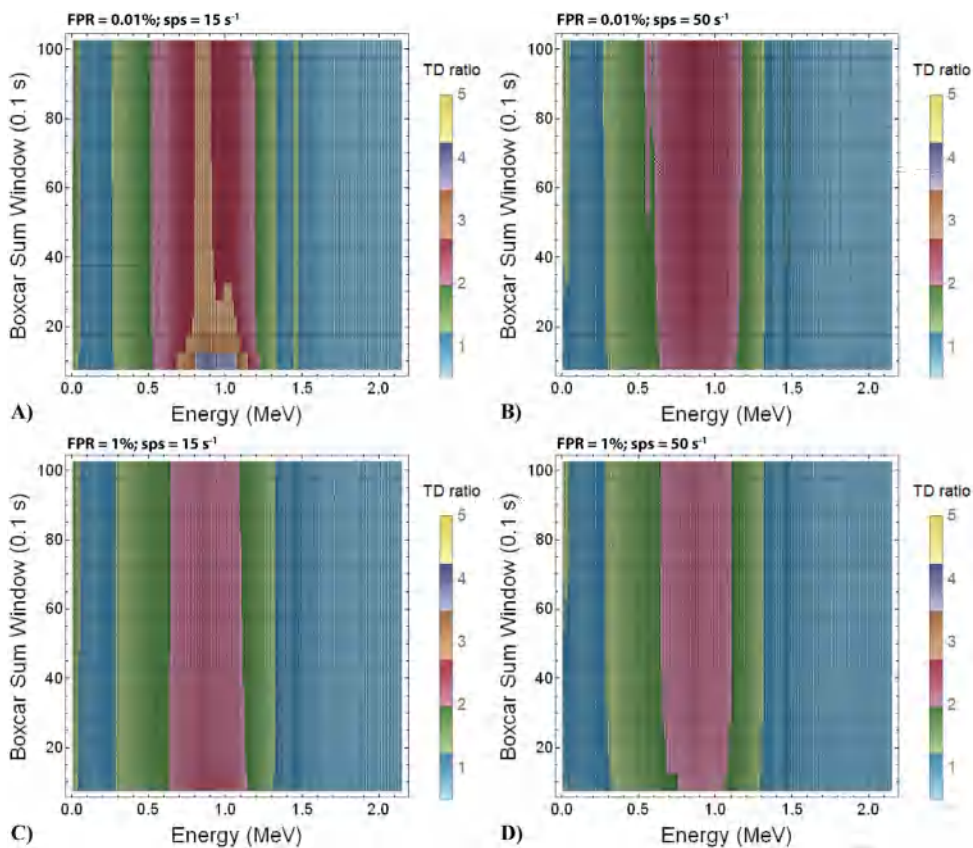


Fig. 5. TTD ratio of KSI-to-NaI(Tl) as a function of the boxcar width and gamma energy. The evaluated source strength is 15 s⁻¹ (A) and (C)) and 50 s⁻¹ (B) and (D)) for a FPR of 0.01% (A)–(B)) and 1% (C)–(D)). The TTD ratio is largest in the region where the 1.31 MeV beta from ⁴⁰K decay dominates, particularly for a FPR of 0.01% and small BCS. (For interpretation of the references to color in this figure legend, the reader is referred to the web version of this article).

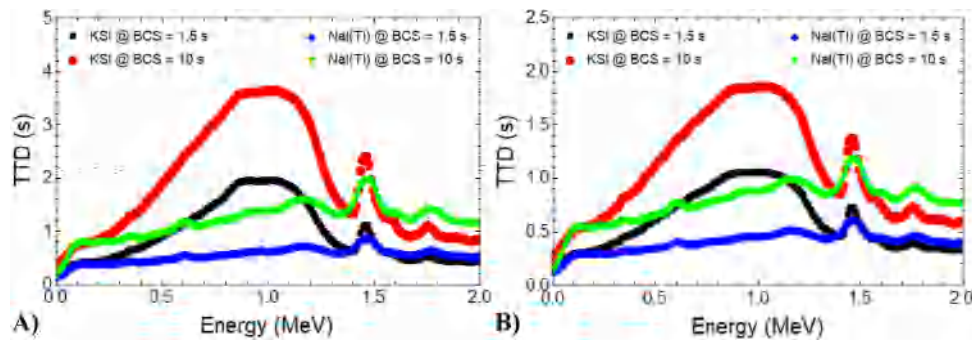


Fig. 6. Comparison of the actual TTD of KSI and NaI(Tl) for a sps of 15 s^{-1} using a BCS of 1.5 s and 10 s and a FPR of (A) 0.01% and (B) 1%. It is apparent that the TTD decreases as the window width decreases, and the TTD of KSI is better than NaI(Tl) where the background from ^{40}K does not dominate the total background observed by KSI. As the FPR is decreased, the TTD of both KSI and NaI(Tl) decrease.

4. Conclusion

In this report, we presented a quantitative comparison via computational analysis of the time-to-detection of single gamma lines for the scintillators $\text{KSr}_2\text{I}_5:\text{Eu}^{2+}$ and NaI(Tl). The lowest time-to-detection was determined by identifying the optimum photopeak integration window for the parameter space (source striking strength, gamma energy, false positive rate, and boxcar window). We found that the optimum integration window was relatively insensitive to the desired false positive rate, but noticeable differences were apparent where the 1.31 MeV beta dominates the observed background in $\text{KSr}_2\text{I}_5:\text{Eu}^{2+}$. The time-to-detection for $\text{KSr}_2\text{I}_5:\text{Eu}^{2+}$ was larger than NaI(Tl) by a factor of one-to-three where the intrinsic background was present, the largest difference occurring between 0.6–1.2 MeV. The time-to-detection difference decreased as the acceptable false positive rate was increased from 0.01% to 1%, and $\text{KSr}_2\text{I}_5:\text{Eu}^{2+}$ was able to identify any single gamma line faster than NaI(Tl) at very low energies ($E_g \lesssim 200 \text{ keV}$) and above the beta end point energy ($E_g \gtrsim 1.3 \text{ MeV}$). Although the parameter space was bounded, the results indicate that there is a global minimum TTD ratio between $\text{KSr}_2\text{I}_5:\text{Eu}^{2+}$ and NaI(Tl) between BCS and sps.

While the results indicate that KSI exhibits a higher time-to-detection than NaI(Tl) in this study, it does not represent a reduced capacity for isotope identification. The results presented merely indicate the expected optimum data acquisition parameters and associated time-to-detection of single gamma lines. Using this technique alone, the time-to-detection of KSI for ^{137}Cs decreases from 0.46 s (662 keV only) to 0.403 s (662 keV and 32 keV), or by 12.4%. Correspondingly, NaI(Tl) decreases its time-to-detection from 0.221 s to 0.210 s when considering both photons from Cs-137, which is only a 5.0% decrease. However, it is demonstrated in the literature that more advanced techniques to isotope identification are available [3,14–19]. Some of these techniques may benefit from the results and / or methodology presented [15–19], and others clearly indicate that the better energy resolution and predictability of the intrinsic background will likely yield more favorable results [3,14]. Considering KSI, further investigation is required to identify the optimum isotope identification technique to maximize its value to the community, and whether its lower cost offsets its intrinsic background compared to other good energy resolution scintillators like $\text{SrI}_2:\text{Eu}^{2+}$.

Acknowledgments

This material is based upon work supported by the U.S. Department of Homeland Security under grant no. 2014-DN-077-ARI088-01. Disclaimer: The views and conclusions contained in this document are those of the authors and should not be interpreted as necessarily representing the official policies, either expressed or implied, of the U.S. Department of Homeland Security.

References

- [1] L. Stand, M. Zhuravleva, A. Lindsey, C.L. Melcher, Potassium strontium iodide: A new high light yield scintillator with 2.4% energy resolution, in: Nuclear Science Symposium and Medical Imaging Conference (NSS/MIC), IEEE, 2013, pp. 1–3.
- [2] L. Stand, M. Zhuravleva, A. Lindsey, C.L. Melcher, Growth and characterization of potassium strontium iodide: A new high light yield scintillator with 2.4% energy resolution, Nucl. Instrum. Methods Phys. Res. A 780 (2015) 40–44.
- [3] K.E. Nelson, T.B. Gosnell, D.A. Knapp, The Effect of Gamma-Ray Detector Energy Resolution on the Ability To Identify Radioactive Sources, United States, 2009.
- [4] T. Burr, M. Hamada, Radio-isotope identification algorithms for NaI γ spectra, Algorithms 2 (1) (2009) 339.
- [5] M. Rust, C. Melcher, E. Lukosi, Intrinsic radioactivity of $\text{KSr}_2\text{I}_5:\text{Eu}^{2+}$, Nucl. Instrum. Methods Phys. Res. A (2016) submitted for publication.
- [6] L.A. Boatner, J.O. Ramey, J.A. Kolopus, R. Hawrami, W.M. Higgins, E. van Loef, J. Glodo, K.S. Shah, E. Rowe, P. Bhattacharya, E. Tupitsyn, M. Groza, A. Burger, N.J. Cherepy, S.A. Payne, Bridgman growth of large $\text{SrI}_2:\text{Eu}^{2+}$ single crystals: A high-performance scintillator for radiation detection applications, J. Cryst. Growth 379 (2013) 63–68.
- [7] N.J. Cherepy, B.W. Sturm, O.B. Drury, T.A. Hurst, S.A. Sheets, L.E. Ahle, C.K. Saw, M.A. Pearson, S.A. Payne, A. Burger, L.A. Boatner, J.O. Ramey, E.V. van Loef, J. Glodo, R. Hawrami, W.M. Higgins, K.S. Shah, W.W. Moses, SrI_2 scintillator for gamma ray spectroscopy, 2009.
- [8] F.G.A. Quarati, I.V. Khodyuk, C.W.E. van Eijk, P. Quarati, P. Dorenbos, Study of ^{138}La radioactive decays using LaBr_3 scintillators, Nucl. Instrum. Methods Phys. Res. A 683 (2012) 46–52.
- [9] F. Quarati, A.J.J. Bos, S. Brandenburg, C. Dathy, P. Dorenbos, S. Kraft, R.W. Ostendorf, V. Ouspenski, A. Owens, X-ray and gamma-ray response of a $2'' \times 2''$ $\text{LaBr}_3:\text{Ce}$ scintillation detector, Nucl. Instrum. Methods Phys. Res. A 574 (1) (2007) 115–120.
- [10] L. Stand, M. Zhuravleva, J. Johnson, M. Koschan, Y. Wu, S. Donald, K. Vaigneur, E. Lukosi, C. Melcher, Exploring growth conditions and Eu^{2+} concentration effects for $\text{KSr}_2\text{I}_5:\text{Eu}$ scintillator crystals II: $\phi 25 \text{ mm}$ crystals, J. Cryst. Growth 483 (2018) 301–307.
- [11] L.M. Stand Stracuzzi, Discovery and Development of Potassium-Based Metal Halide Scintillators for Radiation Detection Applications, 2018.
- [12] J.M. Blackadar, Automatic isotope identifiers and their features, IEEE Sensors 5 (4) (2005) 589–592.
- [13] MCNP6 User's Manual, Version 1.0, Denis Pelowitz, others, Los Alamos, NM, 2008.
- [14] R.C. Runkle, M.F. Tardiff, K.K. Anderson, D.K. Carlson, L.E. Smith, Analysis of spectroscopic radiation portal monitor data using principal components analysis, IEEE Trans. Nucl. Sci. 53 (3) (2006) 1418–1423.
- [15] K.L. Coop, Monte Carlo Simulation of the sequential probability ratio test for radiation monitoring, IEEE Trans. Nucl. Sci. 32 (1) (1985) 934–938.
- [16] P. Luo, T.A. DeVol, J.L. Sharp, Sequential probability ratio test using scaled time-intervals for environmental radiation monitoring, IEEE Trans. Nucl. Sci. 57 (3) (2010) 1556–1562.
- [17] K.D. Jarman, L.E. Smith, D.K. Carlson, D.N. Anderson, Sequential probability ratio test for long-term radiation monitoring, in: 2003 IEEE Nuclear Science Symposium. Conference Record (IEEE Cat. No.03CH37515), 2003.
- [18] J. Stinnett, C.J. Sullivan, H. Xiong, Uncertainty analysis of wavelet-based feature extraction for isotope identification on naI gamma-ray spectra, IEEE Trans. Nucl. Sci. 64 (7) (2017) 1670–1676.
- [19] J. Stinnett, C.J. Sullivan, An automated isotope identification algorithm using Bayesian statistics, in: 2013 IEEE Nuclear Science Symposium and Medical Imaging Conference (2013 NSS/MIC), 2013.